Dynamic Exchange in the Strong Field Ionization of Molecules

Vinay Pramod Majety[*] and Armin Scrinzi[†]

Physics Department, Ludwig Maximilians Universität, D-80333 Munich, Germany

(Received 15 May 2015; published 1 September 2015)

We show that dynamic exchange is a dominant effect in strong field ionization of molecules. In CO_2 it fixes the peak ionization yield at the experimentally observed angle of 45° between polarization direction and the molecular axis. For O_2 it changes the angle of peak emission and for N_2 the alignment dependence of yields is modified by up to a factor of 2. The effect appears on the Hartree-Fock level as well as in full *ab initio* solutions of the Schrödinger equation.

Experimental techniques like molecular orbital tomography [1,2], laser-driven electron diffraction [3,4], and high harmonic imaging [5] are based on the control of ionization by the strong field of a laser. They share the concept that an electron is emitted by a strong laser field and redirected by the same field to its parent system, where it produces a snapshot of the system's time evolution in the angle-resolved electron momentum or harmonic spectra. The analysis of these experiments relies on the idea that the steps of initial electron emission, propagation, and scattering of the returning electron can be considered as largely independent. Adequate understanding of each of these three steps is a prerequisite for proper use of the techniques.

In this Letter we deal with the ionization step. With atoms, there are several models that deliver correct ionization yields at infrared (IR) wavelength. In contrast, for molecules a disquieting discrepancy between theoretical predictions and experiment appeared: two independent experiments at two different intensities [6,7] reported maximal ionization of CO_2 when the molecular axis was aligned at 45° to the polarization direction of a linearly polarized pulse. In contrast, most theoretical calculations found angles in the range 30°–40°.

It is usually assumed that ionization at IR wavelength is a tunneling process and yields can be obtained as the integral over the tunneling rates computed at the instantaneous field strengths. As the field ionization rates drop exponentially with the ionization potential, one expects that the highest occupied molecular orbital (HOMO) in a molecule determines ionization. In particular, the angle dependence of the ionization rate should reflect the electron density distribution of the HOMO. Combining this idea with the Ammosov-Delone-Krainov (ADK) [8] formula for tunneling from effective single-electron systems, the molecular ADK (MO-ADK) approach was formulated [9]. In more complicated molecular systems with energetically closely spaced ionic states this approach may become invalid [5,10]: at the nodal directions of the HOMO, where MO-ADK would show nearly no ionization, the energetically next lower orbital HOMO-1 could contribute. On this level of theory, the discrepancy with experiments [6,7] could not be removed.

A large number of models and computations have been tried to clarify the point. Density functional theory (DFT) calculations indicated that energetically lower molecular orbitals cannot account for the experimental observation [11]. A time-dependent DFT calculation [12] predicts peak yield at 40°. A single electron model with a frozen core potential produced the experimental value of 45° [13]. A coupled channels calculation partially including multielectron effects [14] showed that a single channel picture leads to peak angles ∼30° and it was conjectured that interchannel couplings could explain the experimental observation. A recent time-dependent configuration-interaction (TDCI) calculation using a Gaussian basis expansion [15] in turn reports a peak angle of 50°. Other efforts using the semiclassical WKB approximation [16] and the strong field eikonal Volkov approximation [5] also fail to yield accurate predictions. Recently, it was shown that field distortion of the orbitals plays a role, but the predicted angles of 36° to 39° [17] fall short of the experimental values. In spite of all efforts, the discrepancy remained unresolved.

In the discussion so far, little attention has been paid to exchange symmetry. Ideally, in DFT such effects would be fully included, but in practice this is hardly ever achieved due to limitations of the exchange-correlation potentials. The value of 45° obtained in Ref. [13] using a single electron potential supplemented with a DFT-based exchange correction was attributed to excited state dynamics rather than exchange. The fact that the result is not reproduced by pure DFT using different exchange correlation functionals [11,12] suggests that the agreement may be coincidental. The TDCI of Ref. [15] naturally includes exchange, but in turn the Gaussian expansion is known to have shortcomings in the description of strong-field effects.

In this Letter, we show that dynamic exchange occupies a central place in strong field ionization (SFI). Specifically, in CO_2 exchange forces lead to peak ionization at an alignment of 45°. Effects on the alignment dependence of O_2 and N_2 ionization are sizable but less conspicuous. By

dynamic exchange we designate effects beyond the anti-symmetry of initial and final states. Exchange had been considered for the initial states. In stationary first order perturbative transitions final state antisymmetry can be disregarded for symmetric transition operators. However, omitting antisymmetrization of the virtual states appearing during ionization turns out to constitute, somewhat counterintuitively, an important dynamical restriction. Qualitatively, this will be shown already on the Hartree-Fock level.

We compute SFI rates and solutions of the time-dependent Schrödinger equation (TDSE) by the *ab initio* hybrid antisymmetrized coupled channels (haCC) approach [18]. haCC uses a multielectron wave function in terms of several ionic states $|I\rangle$ that are fully antisymmetrized with a numerical single electron basis, $|i\rangle$. In addition, the neutral ground and excited states $|\mathcal{N}\rangle$ can be included, resulting in the wave function

$$|\Psi_A\rangle = \sum_{i,I} \mathcal{A}[|i\rangle|I\rangle]C_{i,I} + \sum_{\mathcal{N}} |\mathcal{N}\rangle C_{\mathcal{N}}, \qquad (1)$$

which we will refer to as ansatz A in the following. The $C_{i,I}$, $C_{\mathcal{N}}$ are the respective expansion coefficients and $\mathcal{A}$ indicates antisymmetrization. The $|I\rangle$ and $|\mathcal{N}\rangle$ states were obtained from the COLUMBUS quantum chemistry package [19]. For $|i\rangle$ we use a high-order finite element radial basis combined with single center spherical harmonics. A complete description of the method can be found in Ref. [18]. The ansatz accurately describes the single-electron asymptotic behavior, whose importance is discussed in Ref. [20]. Neutral and ionic states can be included to examine multielectron effects like field-free correlation, interchannel coupling and ionic core polarization.

Tunneling ionization rates are computed using exterior complex scaling [21–23]: the Hamiltonian is analytically continued by transforming the electron coordinates into the complex plane. For radii $r > R_0$ one uses $r_\theta = e^{i\theta}(r - R_0) + R_0$ with the complex scaling angle $\theta > 0$. The resulting Hamiltonian is non-Hermitian with a complex ground state eigenvalue $W = E_0 + E_s - (i/2)\Gamma$, where E_0 is the field-free ground state energy, E_s is its dc-Stark shift and $\Gamma/\hbar$ is the static field ionization rate. Apart from errors due to finite computational approximation, W is independent of $\theta > 0$ and $R_0 \geq 0$.

We treat the CO_2 molecule with nuclear positions fixed at the equilibrium C-O bond length of 116.3 pm. The multielectron states of neutral and ion are computed using COLUMBUS with the minimally augmented cc-pvtz basis at the multireference configuration interaction singles level. We used up to 6 ionic channels which include the doubly degenerate $X^2\Pi_g$, $A^2\Pi_u$, and the singly degenerate $B^2\Sigma_u^+$, $C^2\Sigma_g^+$ states. Single electron functions with up to 84 linear coefficients with finite element orders 12 on a radial box of 30 a.u. and up to 269 spherical harmonics

($L_{max} = 12, M_{max} = 12$) were used for the stationary problem. For solutions of the TDSE the number of spherical harmonics was increased up to 324. This numerical basis is complemented by the atom-centered Gaussians that constitute the neutral and ionic functions. For complex scaling, we chose R_0 values well outside the range of neutral and ionic orbitals, such that only the coordinate of the single-electron basis is continued to complex values. Basis and the scaling parameters R_0 and θ were varied to ensure that results are converged to better than 2%. The main approximation is introduced by the limited number of ionic channels. With 6 ionic channels, we obtain a first ionization potential of $I_p = 13.85$ eV (experimental value: 13.78 eV [24]), which decreases by about 0.14 eV with fewer ionic channels.

The central results are shown in Figs. 1, 2, and 6. In Fig. 1, one sees that the static field ionization rates peak at an alignment angle of 45°. Minima appear at 0° and 90° corresponding to the nodal planes of the CO_2 HOMO. These findings agree with experiments [6,7]. Multielectron effects reduce the ionization rates as the number of ionic channels grows: quadratic dc-Stark shifts increase as the basis becomes more flexible. This affects the neutral more strongly than the tightly bound ion and raises the effective ionization potential.

Figure 2 shows the angle of the peak rate as a function of intensity: except for the highest intensities, the angle varies by $\lesssim 2°$, depending on the number of ionic channels included. We cannot confirm any intensity dependence as was predicted in Ref. [16] based on analytic arguments. Dependence on the number of channels is strongest at the higher intensities $I \gtrsim 2.5 \times 10^{14}$ W/cm². There, the tunneling picture ceases to be applicable: according to a simple estimate [23] at intensities $I_b \approx I_p^2/4 = 1.5 \times 10^{14}$ W/cm² the molecular binding barrier of CO_2 is suppressed to
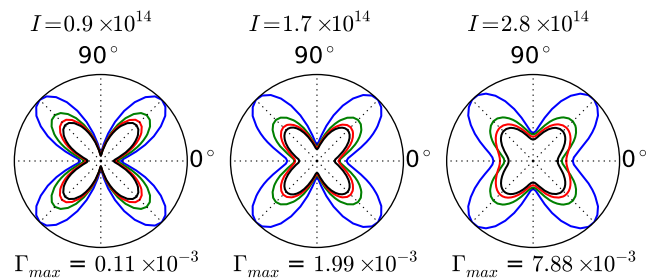

FIG. 1 (color online). Alignment angle dependent CO_2 ionization rates at selected intensities I (in W/cm²). The convergence with the number of ionic channels indicates the role of multielectron effects. Blue: including only the neutral ground state and ionic $X^2\Pi_g$ ground states, green: as blue with the ionic $A^2\Pi_u$ channel added. Red: as green with $B^2\Sigma_u^+$ channel. Black: as red with $C^2\Sigma_g^+$ channel. Computations were performed for static fields of strengths $F = 0.05, 0.07$, and 0.09 a.u. corresponding to intensities $I = F^2/2$ that label the plots. Γ_{max} indicates maximal decay width in atomic units at the inclosing circle. A total of 6 ionic channels are used in the calculations.
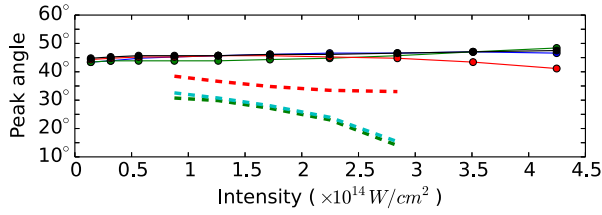
FIG. 2 (color online).   Peak ionization angles as a function of intensity. Solid lines: results with the antisymmetrized ansatz A, Eq. (1). Dashed lines: results without antisymmetrization, ansatz B, Eq. (2). Colors correspond to different numbers of neutral states and ionic channels, see Fig. 1 (solid lines) and Fig. 4 (dashed lines).

below the field free ground state energy. In this regime, virtual continuum states for polarization of the ionic core may become important, which is not modeled by the haCC ansatz as used here and therefore no dependable statement about the accuracy of our results can be made.

The alignment dependence of ionization obtained in quasistatic approximation (QSA) by integrating the tunnel ionization rate is confirmed by solutions of the complete TDSE. In Fig. 3, normalized angle dependent yields obtained from TDSE and QSA within the single channel model are compared with experiments performed at near infrared ($\lambda \approx 800$ nm) wavelength. The angle dependence in TDSE is well approximated in QSA, with better agreement for higher intensities, where the QSA is more appropriate [23]. This agreement is gratifying, considering that in the intensity range $3 \times 10^{13} - 1.1 \times 10^{14}$ W/cm^2 with Keldysh parameters $\gamma = 2 \sim 1$, one can hardly expect ionization to be of pure tunneling type. A failure of the tunneling picture is exposed in the *magnitudes* of the yields, where the TDSE results exceed the QSA by a factor 2 at 1.1×10^{14} W/cm^2 and by nearly 2 orders of magnitude at 3×10^{13} W/cm^2. The fact that angle dependence
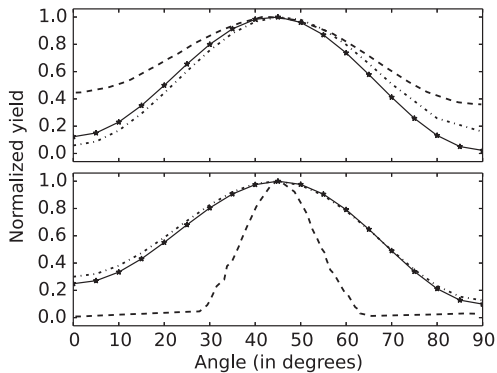

FIG. 3.   Normalized angle dependent yields from TDSE (lines), QSA (dash-dotted lines) in the single channel picture, and experiments [6,7] (dashed lines). The laser parameters are 800 nm central wavelength, 40 fs duration with peak intensities of 3×10^{13} W/cm^2 (Upper panel) and 1.1×10^{14} W/cm^2 (lower panel).

largely agrees between time-dependent and quasistatic ($\lambda \to \infty$) results shows that wavelength effects are secondary compared to exchange. The peak angle is consistent with the experiments, but yields found in one of the experiments [6] are more narrowly confined around the maximum angle. It was noted in Ref. [20] that the experimental result may be artificially narrowed due to the deconvolution procedure.

The failure of earlier theory in reproducing the peak angle of 45° is due to the absence or insufficient inclusion of dynamical exchange. This is clearly seen by omitting from the haCC ansatz A the antisymmetrization of the single-electron basis against the multielectron states in an otherwise identical wave function, ansatz B:

$$|\Psi_B\rangle = \sum_{i,I} |i\rangle |I\rangle C_{i,I} + \sum_{\mathcal{N}} |\mathcal{N}\rangle C_{\mathcal{N}}, \qquad (2)$$

In Fig. 4 one sees that with ansatz B one obtains the peak rate at an angle around 30° at low intensities that then dips off as the intensity is increased; see also Fig. 2.

Our results without antisymmetrization for the dynamics are consistent with Ref. [14], where it was proposed that the remaining discrepancy to the experimental value was caused by neglecting coupling between $X^2\Pi_g$ and $A^2\Pi_u$ ionic channels in the calculation. In contrast, in Ref. [13], the angle near 45° was attributed to dynamics of excited neutral states, mostly the first excited neutral state. However, neither excited state dynamics nor coupling of ionic channels, in the absence of dynamical exchange, result in correct angles.

Figure 4 shows that the first excited state of the neutral has hardly any discernable role in determining the emission profile and does not influence the angle of peak emission. Coupling of channels as proposed in Ref. [14] does move the angle closer to experiment, but still does not yield the correct result. The improvement can be understood as, in the limit of a complete set of channels, ansatz A and B are
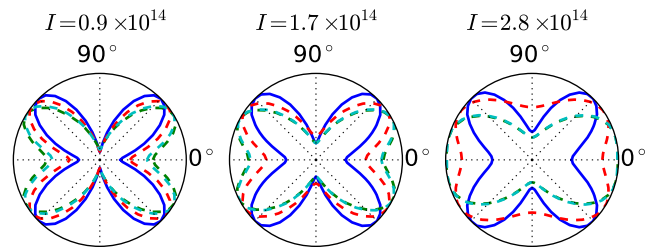

FIG. 4 (color online).   The role of exchange in CO_2 ionization: alignment angle dependence of normalized static SFI rates in different single-channel models. Blue: antisymmetrized ansatz A with the neutral ground state and ionic $X^2\Pi_g$ ground state channels. Green: ansatz B with the same states as blue, red: as green, with the addition of the ionic $A^2\Pi_u$ state. Cyan: as green with the addition of the first excited neutral state. The green and cyan lines coincide at the two higher intensities.

equivalent. However, the primary role of the seemingly complicated multi-electron dynamics is to mimic dynamical exchange. In contrast, with dynamical exchange properly considered, a simple essentially single-electron picture of field ionization reemerges.

We demonstrate this by reducing the problem to the simplest possible case. We use the Hartree-Fock neutral state of CO_2 and the ion ground state in Koopman's approximation. Denoting by $\{\phi_1, \ldots, \phi_N\}$ the occupied Hartree-Fock orbitals of the neutral and by $\psi(t)$ the active electron, ansatz A and B are reduced to

$$|\Psi_A\rangle = \det(|\psi(t)\rangle|\phi_2\rangle \ldots |\phi_N\rangle)C_{11} + |\mathcal{N}\rangle C_{\mathcal{N}} \quad (3)$$

$$|\Psi_B\rangle = |\psi(t)\rangle \det(|\phi_2\rangle \ldots |\phi_N\rangle)C_{11} + |\mathcal{N}\rangle C_{\mathcal{N}}, \quad (4)$$

where det indicates the Slater determinant. The effective Hamiltonians governing the time evolution of $\psi(t)$ for the two cases differ only by the exchange term

$$(V_x\psi)(\vec{r}) = \sum_{k=2}^{N} \phi_k(\vec{r}) \int d^3r' \frac{\phi_k(\vec{r}')\psi(\vec{r}')}{|\vec{r} - \vec{r}'|}. \quad (5)$$

In Ref. [20] it was pointed out that the long-range interactions also affect emission. To exclude those, we smoothly truncate the Coulomb tail of the potential at 10 a.u. Figure 5 shows that also here exchange shifts the peak angle by $\sim 7°$.

Apart from the exchange term, ansatz A effectively enforces orthogonality of the active electron orbital against the ionic HF orbitals $\langle\psi|\phi_k\rangle = 0, k \geq 2$. If this were the dominant effect of antisymmetrization, one would expect that in the absence of the constraint (ansatz B) the ground state energy would be lowered. On the other hand, antisymmetrization effectively enlarges the ansatz space: it operates in the N-fold larger space containing all permutations of ψ through the $\phi_2 \ldots \phi_N$, but including explicitly only the dynamically accessible subspace of antisymmetrized linear combinations. Conversely, omitting antisymmetrization amounts to a restriction of the accessible space.

By this reasoning, Stark-shift (polarization) should be larger in ansatz A. Indeed, we find the latter in our calculations. We also directly verified that an orthogonality constraint on $\psi(t)$ against the ϕ_k in ansatz B causes only $\lesssim 1\%$ of the overall difference between the results of A and B. This finally establishes that indeed the dynamical effects of exchange play the decisive role in ionization.

Dynamical exchange is most conspicuous in CO_2, but the mechanism as such is universal and must be included for obtaining correct ionization rates from any system. As further examples, we studied the effect on N_2 and O_2, which are standard model systems for strong field physics. Figure 6 shows normalized ionization rates at the respective equilibrium nuclear positions with a single channel in ansatz A and B. In N_2, dynamical exchange leads to a broadening of the ionization profile, where the ratio between the rates at 0° and 90° changes by up to a factor ~ 2. For O_2, dynamic exchange shifts the peak angle by 5° to 45° in agreement with the experimental value [6]. Without exchange, our result agrees with the MO-ADK findings and DFT [6,11]. This small discrepancy had not drawn much attention earlier.

In conclusion, we have established that dynamical exchange takes a central place in the ionization of molecules. The effects on CO_2 are striking, but also for O_2 the peak emission angle is affected and for N_2 results can change by up to a factor 2 merely due to exchange. This indicates that dynamical exchange must be considered in any attempt to understand strong field ionization also of more complex multielectron systems. Depending on the system's structure, effects can range from a minor correction to dramatic qualitative changes. Apart from the ionization yields discussed here, the angular distribution of electron emission at fixed alignment may be affected. A critical assessment of the importance of these distributions for rescattering-based attosecond experiments appears in place. On the other hand, simple antisymmetrization may enhance single-electron and single-channel models that have been applied so far, even without the comparatively heavy numerical apparatus used to establish the fact in the present Letter.
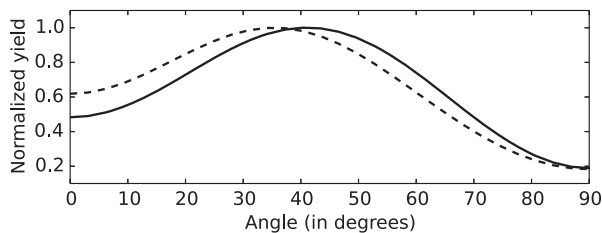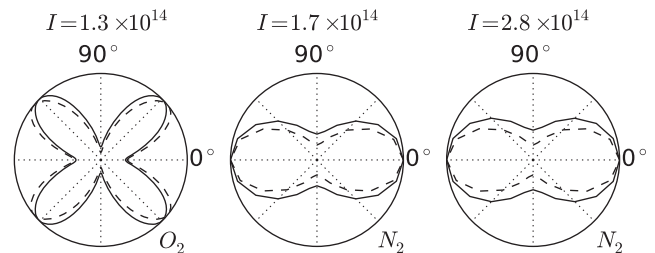

FIG. 5. Rate as a function of alignment, computed with the Hartree-Fock neutral ground state, ionic ground state in Koopman's approximation, and Coulomb potential truncated at 10 a.u. Solid line, with exchange, ansatz A, and dashed line, without dynamical exchange, ansatz B. Field strength = 0.06 a.u.

FIG. 6. Normalized ionization rates of O_2 (left panel) and N_2 (center and right) as a function of alignment angle, using only neutral and ionic ground states. Solid: with dynamic exchange, ansatz A, and dashed, without exchange, ansatz B.

---

[*] vinay.majety@physik.uni-muenchen.de
[†] armin.scrinzi@lmu.de

[1] J. Itatani, J. Levesque, D. Zeidler, H. Niikura, H. Pepin, J. C. Kieffer, P. B. Corkum, and D. M. Villeneuve, Nature (London) **432**, 867 (2004).

[2] P. Salières, A. Maquet, S. Haessler, J. Caillat, and R. Taïeb, Rep. Prog. Phys. **75**, 062401 (2012).

[3] M. Spanner, O. Smirnova, P. B. Corkum, and M. Y. Ivanov, J. Phys. B **37**, L243 (2004).

[4] J. Xu, C. I. Blaga, K. Zhang, Y. H. Lai, C. D. Lin, T. A. Miller, P. Agostini, and L. F. DiMauro, Nat. Commun. **5**, 4635 (2014).

[5] O. Smirnova, Y. Mairesse, S. Patchkovskii, N. Dudovich, D. Villeneuve, P. Corkum, and M. Y. Ivanov, Nature (London) **460**, 972 (2009).

[6] D. Pavičić, K. F. Lee, D. M. Rayner, P. B. Corkum, and D. M. Villeneuve, Phys. Rev. Lett. **98**, 243001 (2007).

[7] I. Thomann, R. Lock, V. Sharma, E. Gagnon, S. T. Pratt, H. C. Kapteyn, M. M. Murnane, and W. Li, J. Phys. Chem. A **112**, 9382 (2008).

[8] M. Ammosov, N. Delone, and V. Krainov, Sov. Phys. JETP **64**, 1191 (1986).

[9] X. M. Tong, Z. X. Zhao, and C. D. Lin, Phys. Rev. A **66**, 033402 (2002).

[10] A. Ferr et al., Nat. Commun. **6**, 5952 (2015).

[11] S. Petretti, Y. V. Vanne, A. Saenz, A. Castro, and P. Decleva, Phys. Rev. Lett. **104**, 223001 (2010).

[12] S.-K. Son and Shih-I. Chu, Phys. Rev. A **80**, 011403 (2009).

[13] M. Abu-samha and L. B. Madsen, Phys. Rev. A **80**, 023401 (2009).

[14] M. Spanner and S. Patchkovskii, Phys. Rev. A **80**, 063411 (2009).

[15] P. Krause and H. B. Schlegel, J. Phys. Chem. Lett. **6**, 2140 (2015).

[16] R. Murray, M. Spanner, S. Patchkovskii, and M. Y. Ivanov, Phys. Rev. Lett. **106**, 173001 (2011).

[17] M. D. Śpiewanowski and L. B. Madsen, Phys. Rev. A **91**, 043406 (2015).

[18] V. P. Majety, A. Zielinski, and A. Scrinzi, New J. Phys. **17**, 063002 (2015).

[19] H. Lischka, T. Müller, P. G. Szalay, I. Shavitt, R. M. Pitzer, and R. Shepard, WIREs Comput. Mol. Sci. **1**, 191 (2011).

[20] S.-F. Zhao, C. Jin, A.-T. Le, T. F. Jiang, and C. D. Lin, Phys. Rev. A **80**, 051402 (2009).

[21] B. Simon, Phys. Lett. A **71**, 211 (1979).

[22] W. P. Reinhardt, Annu. Rev. Phys. Chem. **33**, 223 (1982).

[23] A. Scrinzi, M. Geissler, and T. Brabec, Phys. Rev. Lett. **83**, 706 (1999).

[24] M. Ehara and H. Nakatsuji, Spectrochim. Acta, Part A **55**, 487 (1999).